



# Experimental study on the effect of fine contents on internal erosion in natural soil deposits

Dalang Tian<sup>1,2</sup> · Qiang Xie<sup>1,2</sup> · Xiang Fu<sup>3,4</sup> · Jianhua Zhang<sup>1,2</sup>

Received: 16 November 2018 / Accepted: 27 April 2020 / Published online: 23 May 2020  
© Springer-Verlag GmbH Germany, part of Springer Nature 2020

## Abstract

Seepage-induced internal erosion is observed in both artificially engineered fill structures and natural soil deposits. Fine content is of great significance for the fabric of soil. This paper aimed to determine the critical fine contents of natural soil deposits beyond which the internal stability of the mix was distinctly altered and illustrate the internal erodibility from the viewpoint of fabric. To this end, a fixed-wall permeameter capable of accurately detecting the critical hydraulic gradient of erosion initiation and collecting the cumulative eroded soil mass at a constant inflow rate was developed. Silty clay particles and sandy gravel particles extracted from original soil were employed to reconstitute specimens with fine contents ranging from 0 to 100%. Porosity measurement, seepage testing, and direct shear testing were conducted on remolded samples. Companion control specimens were tested under different flow rates to verify the applicability of the experimental device. The results indicate that according to critical fine content, the fabric of the soil samples with different fine contents could be split into coarse-particle-supported structure (CPSS), fine-particle-supported structure (FPSS), and transitional coarse–fine-particle-supported structure (TCFP). The newly developed experimental device provides a feasible methodology to investigate the internal erodibility of natural soil deposits. Different fabrics correspond to disparate shear strengths and distinct erosion characteristics, including the critical hydraulic gradient of erosion initiation, cumulative eroded soil mass, and average hydraulic conductivity. For coarse-particle-supported structure specimens, the coarse particles predominantly govern the mechanical and hydromechanical properties. An increase in fine content within pores formed by coarse particles could increase shear strength and reduce susceptibility to internal erosion. The mechanical and hydromechanical properties of FPSS specimens were basically controlled by fine particles. Coarse particles suspended in a fine matrix could somewhat increase the soil's shear strength and reduce internal erodibility. TCFP specimens were most vulnerable to internal erosion in terms of minimum critical hydraulic shear stress and maximum cumulative eroded soil mass. It is essential to expand the scope of research to cover the transitional coarse–fine-grain-supported structure instead of remaining limited to the coarse-grain-supported structure.

**Keywords** Internal erosion · Internal stability · Fine content · Natural soil deposits

## Introduction

Internal erosion of soil refers to the process whereby fine particles are detached from a soil structure to the liquid stream flowing through the soil pores and subsequently migrate with the liquid phase. Detached fine particles flowing with the liquid stream will either be entrapped at the pore constrictions or escape from the exit surface without capture. Internal erosion can be initiated by concentrated leak erosion, backward erosion, soil contact erosion, or suffusion (Fry 2012; Fell and Fry 2013; Chang and Zhang 2011). Once the fine particles are removed, the microstructure, hydraulic properties, and mechanical properties change accordingly. Chronic internal erosion will induce a reduction of soil shear strength (Schuler

✉ Qiang Xie  
xieqiang2000@163.com

<sup>1</sup> School of Civil Engineering, Chongqing University, Chongqing 400045, People's Republic of China

<sup>2</sup> Key Laboratory of New Technology for Construction of Cities in Mountain Area, Chongqing University, Chongqing 400045, People's Republic of China

<sup>3</sup> School of Hehai, Chongqing Jiaotong University, Chongqing 400074, People's Republic of China

<sup>4</sup> Changjiang River Scientific Research Institute of Changjiang Water Resources Commission, Hubei 430010, People's Republic of China

1995; Scholtes et al. 2010; Muir Wood et al. 2010) and change of local and/or general hydraulic conductivity properties of the soil (Mehdizadeh et al. 2017; Liu et al. 2019).

Indeed, numerous soil structure failures reported in the literature have been attributed to soil erosion. Seepage-induced erosion plays a significant role in the stability of earth structures, such as dikes, dams, and canals, nearly half of the dysfunction of which is related to internal erosion associated with pore fluid flow (Foster et al. 2000; Fell et al. 2003; Zhang and Chen 2006; Chang and Zhang 2010). This process is not only observed in artificially engineered fill structures but also in natural geomaterials such as natural soil deposits and weathered rocks (Bonelli 2013; Hencher 2006; Hencher 2010; Pepe et al. 2019). Alluvial soil deposits may be eroded by seepage force generated by water leakage from buried pipes and sewage disposal wells, resulting in damage to structures (Khaksar Najafi and Eslami 2015). Based on site investigation, laboratory model tests, and numerical analysis, it has been concluded that under rainfall infiltration, fine particles in natural terrain slopes migrate from the upper part to the toe by interflow, which is vital to trigger slope failure (Crosta and di Prisco 1999; Zhang et al. 2019; Dai et al. 2019). These macro-scale soil structure failures caused by internal erosion demonstrate the urgency of further research on general seepage-induced erosion phenomena in natural soil deposits.

A host of variables play significant roles in the internal erodibility of soil, including the hydraulic gradient, grading curve, fine content, and stress state. The critical hydraulic gradient and/or critical hydraulic shear stress were investigated by substantial research (Khilar and Fogler 1998; Wan and Fell 2004a, b, 2008) to determine the initiation and progression of internal erosion. By means of introducing the “filter” concept, whereby the coarser fraction serves as a filter if water flows through, a variety of empirical methods have been proposed based on the characteristics of the grain size distribution curve (Kezdi 1979; Kenney and Lau 1985; Burenkova 1993; Chang and Zhang 2013). To reveal the impact of stress state on the conditions at onset of instability, a series of new experimental devices were developed based on ordinary triaxial apparatus to control stress on test specimens subjected to internal erosion (Bendahmane et al. 2008; Chang and Zhang 2011; Luo et al. 2012; Slangen and Fannin 2017). However, only a few studies on the internal erodibility of soil have been conducted from the viewpoint of fabric. The fabric here represents the composition of soil, the spatial arrangement of particles, particle groups, and pore spaces (Mitchell and Soga 2005). The fabric varies depending on the initial fine content and preparation method of the specimens.

The initial fine content actually characterizes the effect of soil packing, which may offer a physical explanation for the soil hydromechanical behavior. Kenney and Lau (1985) reported that the maximum content of loose particles that a granular material can contain is an

important factor related to internal erodibility. Similarly, Skempton and Brogan (1994) suggested that a further key to understanding the nature of internal erodibility is the critical content of fines, below which the fine particles do not completely fill the voids within the coarse component; otherwise, the coarse particles float in a matrix of fine particles. Wan and Fell (2008) summarized that one of the three criteria necessary for suffusion in sand–gravel soils is that the amount of fine particles must be less than enough to fill the voids of the basic skeleton formed by the coarse particles. Ke and Takahashi (2012, 2014b) and Ouyang and Takahashi (2015) researched the effect of fine content on suffusion characteristics and the mechanical consequence of specimens subjected to suffusion. In the above studies, the researchers realized the importance of the fine content, the variance of which is likely to change the soil structure, further affecting the mechanism of internal erosion. However, the fine content of all of the reconstituted specimens was less than critical fine content reported by Skempton and Brogan (1994). Furthermore, the specific reason why the selected fine content is limited below the critical fine content was not provided in these studies. In practice, the fine content of natural soil deposits is usually larger than the critical fine content, because of the complexity of the geological processes. To date, few studies have referred to the internal erodibility of soil in which the fine content is larger than the critical fine content mentioned above. Comprehensive interpretation and assessment of the effect of fine content on the internal erodibility of natural soil deposits from the viewpoint of fabric should be performed.

This paper is intended to illustrate experimentally the critical fine content necessary for suffusion of natural soil deposits and to shed light on the effect of fine content on the internal erosion mechanism of soil subjected to pore–fluid flow from the viewpoint of fabric. Because of the absence of a standardized test method, a new fixed-wall permeameter was developed, through which the initiation and evolution of internal erosion within the tested specimens could be observed. By means of the newly developed permeameter, a series of seepage tests were performed on specimens with different fine contents. Direct shear tests were conducted on companion specimens to improve knowledge of the role of fabric in internal erosion. Greater understanding of the effect of fine content on the internal erodibility of natural soil deposits can facilitate explanation of the mechanism of internal erosion and also help geotechnical engineers to assess the potential of internal erodibility of natural soil deposits, especially for widely graded coarse-grained soils with cohesive particles.

## Experimental setup and tested material

### Experimental setup

To investigate the onset and progression of internal erosion induced by pore–fluid flow in reconstituted specimens, a newly experimental setup developed by the authors was designed for broadly graded natural soil deposits with particles from clay to gravel size. The experimental apparatus is a fixed-wall permeameter cell that allows flow through the samples within the cell downward and collection of effluent water containing eroded soil grains. In previous works, most rigid wall permeameters designed to investigate internal erosion have used the constant hydraulic gradient control method (Kenney and Lau 1985; Skempton and Brogan 1994; Moffat and Fannin 2006; Wan and Fell 2008; Ke and Takahashi 2012). In the constant hydraulic gradient control method, the inlet hydraulic pressure is usually maintained by means of a pressurized tank. For natural soil deposits with comparatively high permeability, the test time is strictly restricted by the volume of the water tank. However, because internal erosion is a chronic phenomenon (it usually takes years in nature), a prolonged test time is necessary. Meanwhile, the hydraulic gradient needed by natural soil deposits to trigger and maintain internal erosion is relatively small. It is difficult to control hydraulic pressure and approximate the hydraulic head loss in tubes, valves, and fittings precisely. To avoid these defects mentioned above, the device in this laboratory investigation used the constant flow rate control method instead, which has been effectively demonstrated by some apparatus (Richards and Reddy 2010; Liu et al. 2019). A schematic illustration and photograph of the entire setup are shown in Fig. 1a and b, respectively. Figure 2 shows a schematic diagram of the profile of a permeameter cell.

De-aired water stored in the upper reservoir, which was placed on an electronic balance and was large enough to ensure sufficient water supply, was successively injected into the standing pipe with the same diameter as the sample, through a peristaltic pump. To limit the maximum hydraulic gradient applied to the specimens, an overflow pipe connected to the lower reservoir placed on an electronic balance was installed near the top of the standing pipe. During seepage testing, the two water tanks were weighed continuously to estimate the upward hydraulic pressure. When downstream of the specimen was opened to the atmosphere, the downstream pressure was zero.

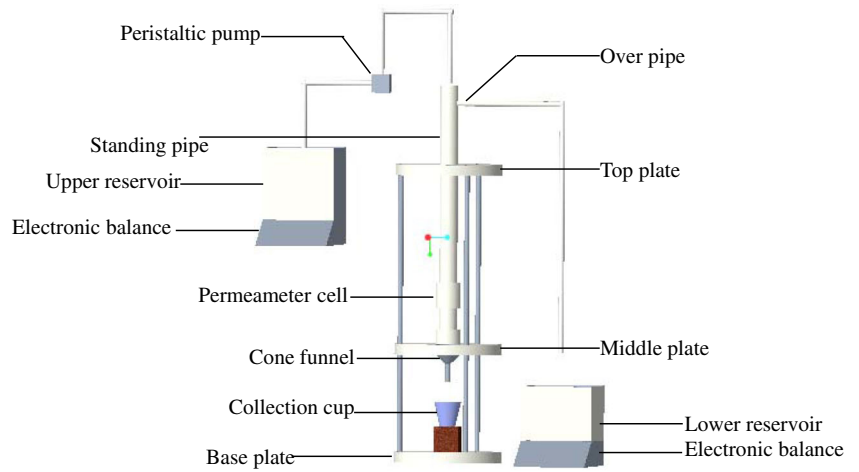
A fixed-wall permeameter cell composed of transparent acrylic pipe accommodated a specimen of 39.1 mm in diameter and 100 mm in height. A conventional fixed-wall permeameter involves the formation of large seepage channel between the compacted specimen and the rigid wall of the permeameter (Kenney and Lau 1985; Bendahmane et al. 2008). A rubber membrane was attached against the inside wall of the permeameter to avoid unexpected parasitic flow.

Glass beads with diameters of 3 mm were used to uniformly circle the fluid coming to the upper surface of the tested sample. A perforated plate with an opening size of 1 mm was attached to the top of the specimen to support the weight of the glass beads and eliminate their effect on the erosion behavior of the tested specimens. To prevent fines loss from the upper surface of the specimen, a nonwoven geotextile was attached between the perforated plate and the upper surface of the specimen. A perforated plate with an opening size of 5 mm was set into the depressed platform on the top of the pedestal to support the tested sample, and its openings, with diameters of 5 mm, allow for investigation of the erosion of most particles within the specimen. Effluent with eroded soil grains flowing through the downstream perforated plate was collected in numbered containers by the inverted cone funnel for further analysis, as designed to prevent the effluent from blocking the drainage system. To decrease the duration of the test, instead of oven drying the effluent to weigh the eroded grains, a glass filter (Fig. 3) was used, with the aid of a vacuum pump. The designed fixed-wall permeameter has been described in detail by Tian (2018).

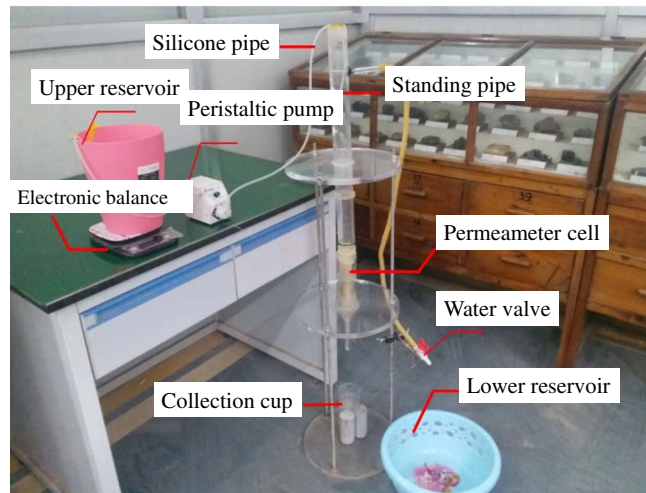
### Tested material

The experimental material used to reconstitute the soil column was collected from slopes consisting of natural soil deposits in Fengjie County, Chongqing, China, where obvious settlement deformation of buildings has resulted from internal erosion induced by intense rainfall (Tian 2018). The natural soil deposits are composed of calcareous marl fragments with diameters ranging from 0.25 mm to 20 mm and silty clay with diameters ranging from 0.002 mm to 0.075 mm, as shown in Fig. 4a. The collected natural soil deposits contain grain diameters varying mainly from 0.002 mm to 20 mm. Particles with diameters larger than 10 mm were removed prior to sample preparation, as the diameter of each specimen for the seepage tests was 39.1 mm, as mentioned above. The material tested in the laboratory investigation contained pure silty clay particles and pure sandy gravel particles, as shown in Fig. 4b, which were completely extracted from the original soil by wet sieving (ASTM C117-17 2018). The pure sandy gravel particles were classified as angular to sub-angular material. Following standard test method (ASTM D854-14 2018), the grain density of pure sandy gravel particles was identified as  $2.65 \times 10^3 \text{ kg/m}^3$ . The plasticity limit, liquidity limit, and standard optimum water content of the pure separated silty clay particles were 25%, 57.2%, and 27.2%, respectively, based on standard test methods (ASTM D4318-17e1 2018; ASTM D698-12e2 2018). According to ASTM D854-14, the grain density measured for silty clay particles was  $2.63 \times 10^3 \text{ kg/m}^3$ . The grain sizes of the pure sandy gravel particles and pure silty clay were within the ranges 0.25–10 mm and 0.002–0.075 mm, respectively, with particles between 0.075 and

**Fig. 1** Experimental device. **a** Schematic illustration of the entire setup. **b** Photo of the entire setup



(a) Schematic illustration of the entire setup



(b) Photo of the entire setup

0.25 mm in deficiency. The grain size distributions of the original soil, pure sandy gravel, and pure silty clay are shown in Fig. 4c. According to the Unified Soil Classification System (ASTM D2487-11), the original soil is described as SP.

It is important to emphasize that many researchers have pointed out that the grain size distributions of soil can be divided into coarse components making up the primary fabric, which carry the majority of the overburden, and fine

**Fig. 2** Schematic diagram of the profile of a permeameter cell

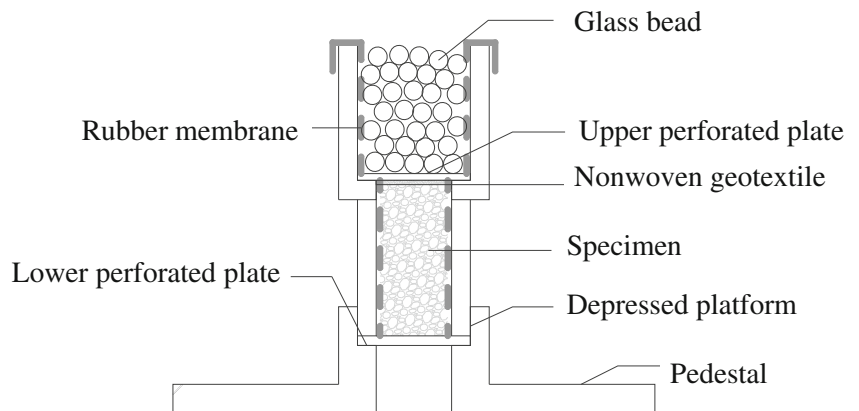
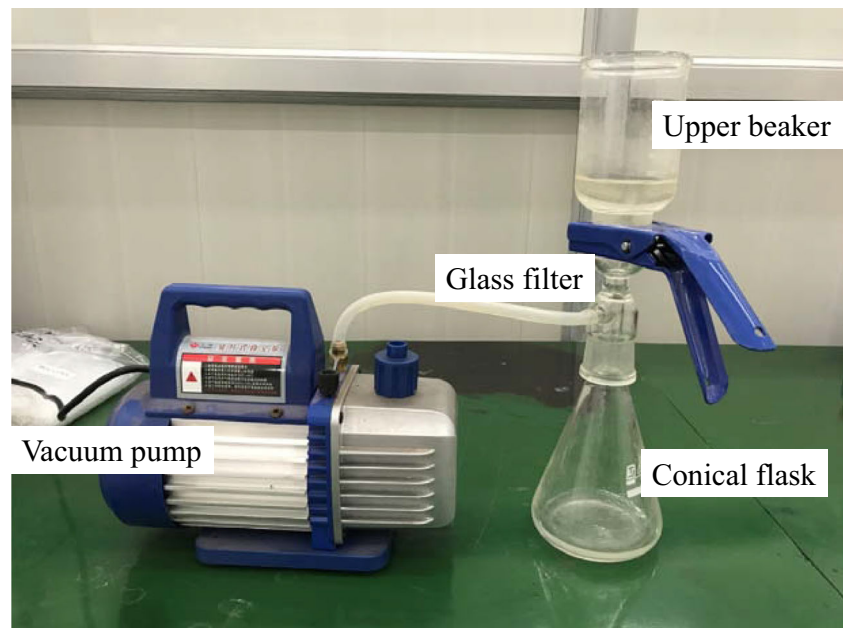


Fig. 3 Photo of filter device



components constituting a secondary structure that bears a smaller amount of the effective stress (Skempton and Brogan 1994; Xiao and Shwiyhat 2012; Ke and Takahashi 2014a, b). However, none of the studies mentioned above defined a specific critical grain size to separate fine components and coarse components in the grain size distribution. Tested specimens in those investigations were usually binary mixtures of two types of granular materials with distinctly different dominant grain sizes. Nonetheless, there was a common characteristic between their tested samples: all of them were gap graded, and the grain sizes of deficient particles were regarded as the critical grain size mentioned above. In accordance with their determination, in this contribution, the silty clay particles with sizes below 0.075 mm were deemed to be fine particles, and the sandy gravel particles larger than 0.25 mm were deemed to be coarse particles.

## Test procedure

The laboratory investigation described in this paper was intended to survey the influence of initial fine content on the mechanism of internal erosion. Therefore, the main testing procedures included preparation of remolded samples with different fine contents, porosity measurement testing, direct shear testing, and erosion testing. A detailed description of each test procedure is presented in the following sections.

## Specimen preparation

A parametric study was conducted in a series of seepage tests. The initial fine content was exclusively studied in this contribution, with other factors that play crucial roles in the internal

erosion kept constant. For each fine content, five specimens were prepared, one of which was intended to conduct the erosion test after porosity measurement, whereas the others were intended to perform direct shear tests under different normal forces. Three additional companion control specimens with an initial fine content of 30% were simultaneously reconstituted to verify the applicability of the newly developed experimental device. The detailed experimental program is presented in Table 1. To avoid particle segregation during preparation, the moist tamping method (Ladd 1978; Frost and Park 2003) was employed. Each sample for the erosion tests was 39.1 mm in diameter, 80 mm in height, and 169 g of target dry weight, and the whole preparation process involved two test procedures: (1) material mixture and (2) specimen compaction.

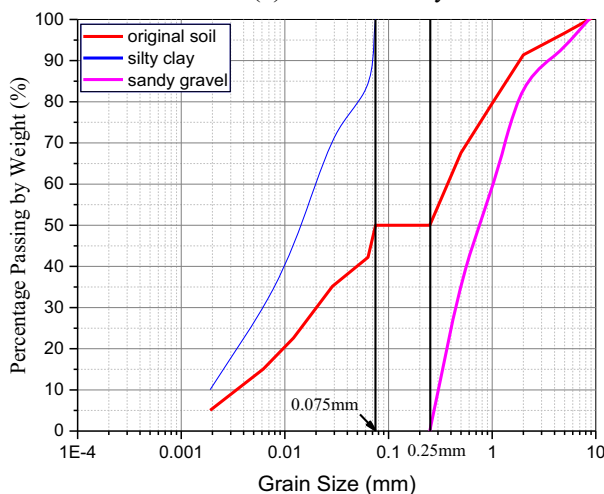
- (1) The oven-dried sandy gravel particles were mixed adequately with de-aired water to a water content of 5%. The role of the water was to prevent the soil from reaching too high density as it was laid out (Andrianatrehina et al. 2016). While mixing continued, fine particles with optimum moisture content, weighted precisely based on the target fine content and target dry weight, were gradually added into the mixture. Mixing was carried out until the mixture appeared visually homogeneous. Thereafter, the well-mixed mixture was preserved in a sealed bag for 24 h before compaction to achieve moisture equalization.
- (2) Samples were compacted manually in five layers under identical compactive effort. The accurately weighed mixture was carefully deposited into the compaction mold with a spoon, and each layer was then compacted with predetermined compactive effort. The detailed characteristics of the reconstituted specimens are summarized in



(a) In the sample site



(b) In the laboratory



(c) Grain size distribution of the test material

**Fig. 4** Granulometric and textural features of the tested material **a** in the sampling site and **b** in the laboratory. **c** Grain size distribution of the tested material

Table 1. It is worth noting that the heights of specimens S9 and S10 exceeded the height of the mold during the process of compaction and the excess portion was removed, resulting in reduction of the target dry weight.

### Porosity measurement test and direct shear test

A steel ruler with a precision of 1 mm was used to measure the height of each reconstituted specimen. Given the height, the porosity of a specimen can be obtained based on the following equation:

$$n_{\text{mix}} = \frac{V_0 - V_S}{V_0} = \frac{V_0 - \left( \frac{w_c}{\rho_c} + \frac{w_f}{\rho_f} \right)}{V_0} \quad (1)$$

where  $V_0$  is the total volume of the reconstituted specimen;  $V_S$  is the volume of grains;  $w_c$  and  $w_f$  are masses of coarse particles and fine particles, respectively; and  $\rho_c$  and  $\rho_f$  are the grain density of coarse particles and fine particles, respectively.

Prior to the erosion tests, a series of direct shear tests under consolidated drained conditions were conducted on companion specimens to determine the role of the fabric of specimens with different fine contents from the viewpoint of mechanical properties. The shear box accommodated circular specimens with a diameter of 61.8 mm and thickness of 20 mm. Reconstituted specimens for direct shear tests were prepared using the same compaction, water content, and mass density as those of specimens prepared for the erosion tests. Specimens were molded by tamping each layer until the accumulative mass of the soil placed in the shear box was compacted to a known volume. Prior to the addition of material for the next layer, the top of each layer shall be scarified. Each reconstituted specimen was sheared under four levels of normal stress, 100, 200, 300, and 400 kPa, at a rate of displacement of 0.8 mm/min. The detailed testing procedure was in accordance with ASTM D3080 2018.

### Erosion test

Finally, specimens were installed into the newly developed rigid wall seepage test device to conduct the seepage erosion tests. Once every system unit was ready, the peristaltic pump was turned on, and de-aired water was injected to the standing pipe at an extremely low-constant inflow rate to saturate the specimen. An extremely low-inflow rate can prevent the migration of particles caused by interflow during saturation. When the discharge rate was stable, the specimens were basically saturated. Thereafter, the peristaltic pump was adjusted to a predetermined constant inflow rate to initiate the erosion test. The effluent was collected over predetermined elapsed time intervals with shorter intervals at first and longer intervals as the test progressed. The effluent was allowed to drip into

**Table 1** Main characteristics of reconstituted specimens

Number of sample	Dry weight (g)	Porosity	Flow rate (ml/min)	Fine content (%)	Dry density (g/cm <sup>3</sup> )	Initial permeability (cm/s)	Critical hydraulic gradient (m/m)
S1	168.3	0.35	/	0	1.80	/	/
S2	168	0.31	78	10	1.81	0.024	0.69
S3	169.5	0.28	78	20	1.88	0.022	0.78
S4	168.9	0.25	78	30	1.97	0.016	0.90
S4-1	168.4	0.24	25	30	1.98	0.014	1.12
S4-2	167.7	0.25	39	30	1.96	0.013	1.0
S4-3	168.1	0.25	56	30	1.97	0.017	1.13
S5	169.3	0.26	78	40	1.96	0.008	1.58
S6	168.6	0.28	78	50	1.89	0.003	2.13
S7	169	0.29	78	60	1.85	0.00074	2.95
S8	168.8	0.32	78	70	1.77	0.0002	5.52
S9	164.8	0.34	78	85	1.72	0.00019	5.9
S10	157	0.38	78	100	1.64	0.0002	6.18

numbered containers. At the end of the elapsed time interval, the weight of the upper reservoir and lower reservoir were recorded, and inlet hydraulic pressure was calculated from the measured weight of the upper and lower reservoirs. The erosion tests were continued until the following criteria were satisfied: (1) the effluent was observed to be visually clear over a period of at least 30 min and upstream hydraulic pressure remained stable; (2) the water table in the standing pipe declined drastically to zero or a minimal value; (3) the duration of test exceeded the specified time of 2 h.

To collect the eroded soil grains within the effluent as quickly as possible, a glass filter was employed with the assistance of a vacuum pump. After filtering, the eroded particles remained on the filter paper while the effluent water permeated to the conical flask. The mass of eroded soil grains and effluent water in each interval could be measured through weighing oven-dried filter papers and the conical flask, respectively.

## Test results and discussion

A parametric study was conducted on this series of tests to illustrate the internal erosion mechanisms of specimens with different fabrics. First, the fabrics of tested specimens were classified according to the measured porosity. Prior to performing the parametric study, the performance of the newly developed device was verified via a series of comparative trials. Then, the evolution of internal erosion with respect to the fine content was described by interpreting the critical hydraulic gradient of erosion initiation, cumulative eroded soil mass, and average hydraulic gradient. Finally, the shear strength and critical hydraulic shear stress were imported to gain further understanding of the internal erosion.

## Classification of the granular structure of tested specimens

To gain an understanding of the particle packing characteristics of the tested specimens with various fine contents and further interpret their effects on internal stability, the fabrics of tested specimens were classified based on the laboratory porosity–fine-grain concentration relationship and the theoretical porosity–fine-grain concentration relationship, referring to methods proposed by Vallejo (2001). A schematic diagram of the fabrics of mixtures consisting of coarse and fine particles of various proportion is shown in Fig. 5. Figure 6 exhibits the changes in porosity undergone by the tested specimens.

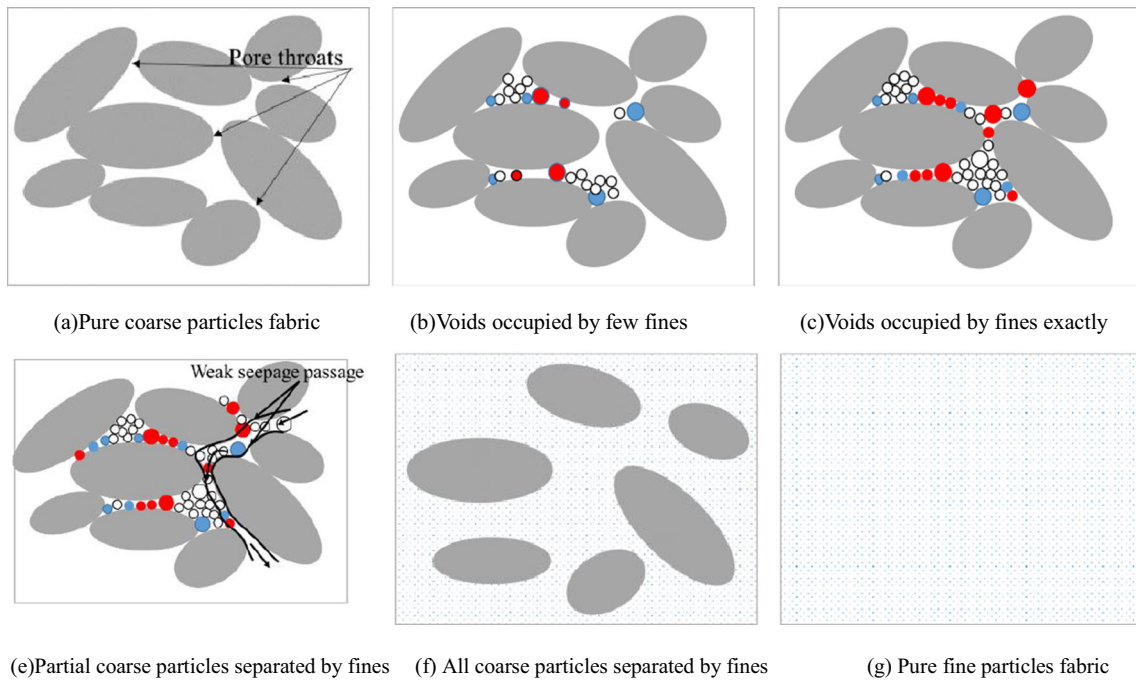
Figure 5a represents the case in which the primary fabric is composed solely of coarse particles, corresponding to point A in Fig. 6 at which the concentration of fines is zero. Similarly, the primary fabric in Fig. 5g corresponds to point F in Fig. 6 at which the concentration of fines is 100%.

Figure 5c shows the case in which the voids between coarse particles are completely occupied by fines, corresponding to point C given in Fig. 6 in which the vertical coordinate represents the theoretical minimum porosity calculated by production of the porosity of coarse particles  $n_c$  and the porosity of fine particles  $n_f$ . The associated horizontal ordinate value represents the theoretical critical fine content  $S_f$  determined through the following equation (Skempton and Brogan 1994):

$$S_f = \frac{n_c(1-n_f)\rho_f}{n_c(1-n_f)\rho_f + (1-n_c)\rho_c} \quad (2)$$

where  $\rho_c$  and  $\rho_f$  are the grain densities of coarse and fine particles, respectively.

Accordingly, points on the theoretical straight line AC in Fig. 6 are related to the state represented in Fig. 5b; that is, fine



**Fig. 5** Schematic diagram of fabric of mixtures with various fine contents. **a** Pure coarse-particle fabric. **b** Voids occupied by few fines. **c** Voids occupied by fines exactly. **d** Partial coarse particles separated by fines. **e** All coarse particles separated by fines. **f** Pure fine particles fabric

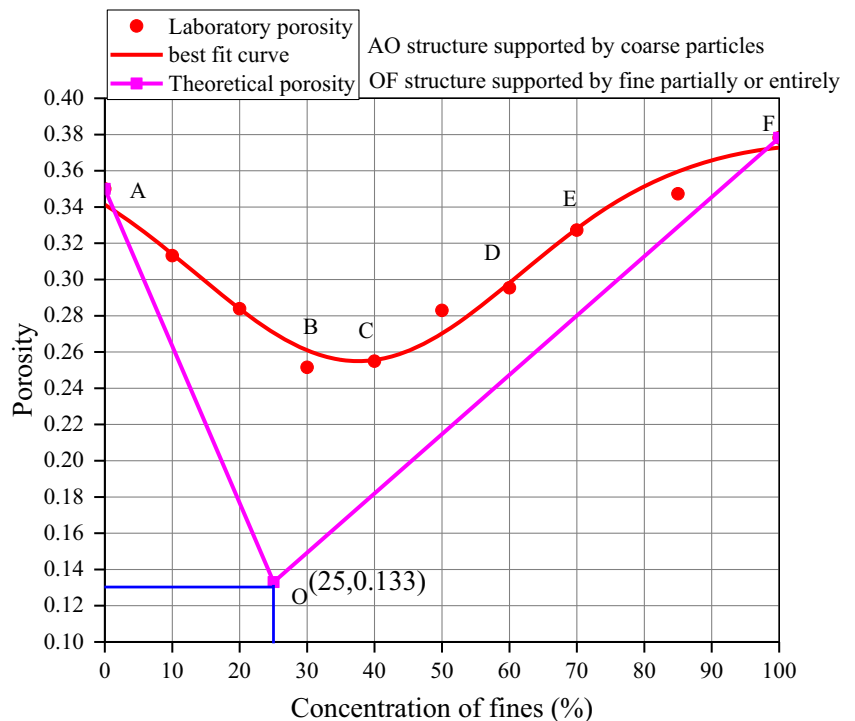
particles exist in the voids between coarse particles. Points on the theoretical straight line OF in Fig. 6 are related to the state represented in Fig. 5e and f: coarse particles separated partially or entirely by the fine-particle matrix.

The obvious gap between the theoretical relationship depicted by the straight line segments AOF in Fig. 6 and the experimental data represented by curve ABF in Fig. 6

demonstrates the difficulty in compacting specimen to the theoretical state. Vallejo (2001) pointed out that a greater degree of compaction could shrink the unexpected gap.

The experimental porosity curve in Fig. 6 indicates that the variation tendency of porosity developed by the tested specimens was in accordance with the theoretical solution, even though the critical fine content and associated minimum

**Fig. 6** Changes in porosity developed by tested specimens with different fines content (points A–F are representative of laboratory porosity; point O is representative of minimum theoretical porosity)





porosity were theoretically identified as 25% and 0.133, whereas they were experimentally identified as within the ranges of 30–40% and 0.25–0.26, respectively. It was easy to clearly distinguish the distinctive critical fine contents used to classify the granular structure of the tested specimens in the experimental data. In this contribution, fine contents of 30% and 70% were chosen to serve as the critical fine contents to divide the granular structure of the tested specimens into three different fabrics, in contrast with fine contents of 40% and 70% proposed by other researchers (Vallejo 2001; Fragaszy et al. 1992). Specimens were classified as coarse-particle-supported structure (CPSS) for fine contents less than 30%, fine-particle-supported structure (FPSS) for fine contents more than 70%, and transitional coarse–fine-particle-supported structure (TCFP) for fine contents from 30% to 70%. The difference between the critical fine contents adopted here and those of Vallejo (2001) are principally attributed to the constituent materials adopted. Specimens in the present study consisted of graded particles separated from original soil, whereas two types of glass beads with different dominant grain sizes were adopted in the study conducted by Vallejo (2001). The reasonableness of the categorization method applied in this study can also be verified by the results of the direct shear tests and erosion tests described below.

### Verification of the newly developed device

The erodibility of soil can be quantified in terms of the critical hydraulic gradient required to initiate internal erosion (Wan and Fell 2004b) and cumulative eroded mass (Bendahmane et al. 2008). The critical hydraulic gradient of erosion initiation quantifies the ease of initiating erosion in the soil; in other words, a higher critical hydraulic gradient implies that a specimen is less vulnerable to internal erosion. The cumulative weight of eroded soil particles measures the extent of damage induced by internal erosion; high cumulative weight of eroded soil particles indicates serious damage formed within specimens. Therefore, it was necessary to verify the capability of the new device developed in this paper to capture the critical hydraulic gradient and cumulative eroded mass accurately. Verification of the newly developed device was carried out through a series of erosion tests conducted on sample S4 and its companion specimens S4-1, S4-2, and S4-3, which had identical fine content of 30%, under different inflow rates (Table 1). Figure 7a plots the cumulative mass of eroded soil grains as a function of the duration of the tests, whereas Fig. 7b displays the cumulative mass of the eroded particles versus the corresponding hydraulic gradient across the specimen. The constant inflow rates applied in each test are specified in the legend.

It was noted that a lower inflow rate could delay the erosion initiation and reduce the extent of internal erosion, demonstrated by lower cumulative mass over the same test duration

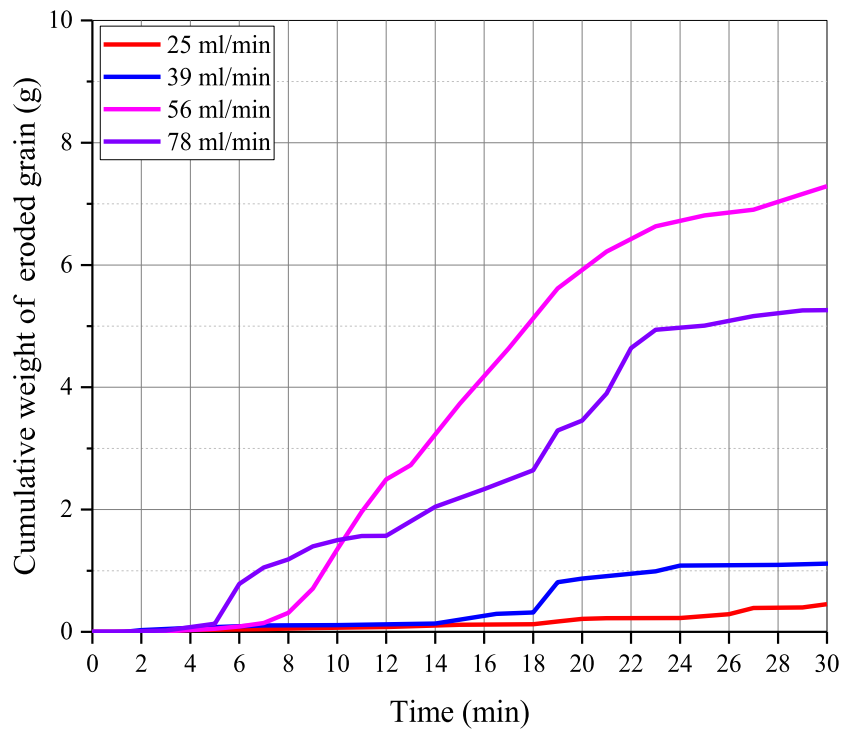
(Fig. 7a). It is easy to shed light on this observation. In four tests conducted on identical samples under different inflow rates, a greater inflow rate could result in higher inlet hydraulic pressure, which is crucial to internal erosion, over the same interval of time, compared with a lower inflow rate. Analysis of the cumulative weight of eroded soil versus the hydraulic gradient curve indicates that the critical hydraulic gradients of erosion initiation ( $i_{sat}$  in Fig. 7b) detected in these tests were nearly identical. The critical hydraulic gradients measured in these four tests were 0.90, 1.12, 1.0, and 1.13 m/m, as shown in Table 1, with a mean value of 1.04 m/m and a standard deviation of 0.094. The consistency of the critical hydraulic gradient of erosion initiation confirms the capability of the newly developed device to conduct erosion seepage investigation on natural soil deposits. Figure 7b also shows that the portion in the curve subsequent to the initiation of internal erosion was obviously affected in these four tests. This effect can be attributed to numerous factors including the topology of the pore network and the inhomogeneity of the samples (Xiao and Shwiyhat 2012; Reddi and Bonala 1997).

### Erosion characteristics

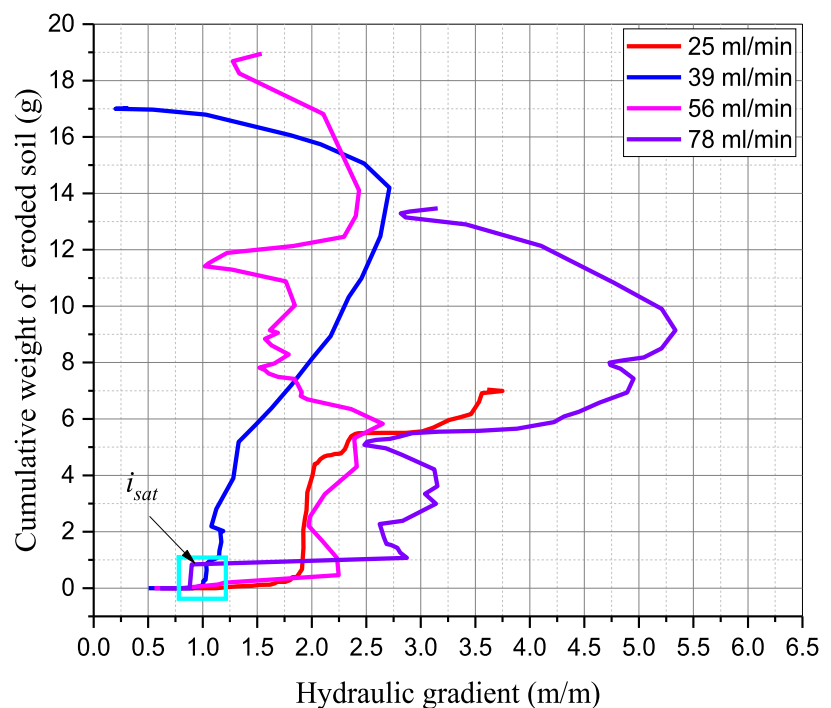
In addition to the critical hydraulic gradient of erosion initiation and cumulative weight of eroded soil particles discussed above, the average hydraulic conductivity, which was estimated during the seepage tests based on the assumption that the seepage flow pattern was laminar and followed Darcy's law, is reported. This parameter is intended to elaborate the erosion mechanism of specimens with various fine contents from the viewpoint of the influence of the fabric on hydraulic properties. The evolution of erosion characteristics including the critical hydraulic gradient of erosion initiation, cumulative weight of eroded soil particles, and average hydraulic conductivity with respect to the concentrations of fines are plotted in Fig. 8a, b, and c, respectively. Specimens with fine contents of zero could not be transferred from the compaction mold to the permeameter cell intact because of weak interparticle bonding; therefore, erosion tests cannot be conducted on such samples. For specimens with initial fine contents of 50% and 100%, collapse of samples took place during the seepage erosion tests. Their eventual cumulative weights of eroded soil particles (39.6 g and 38.7 g, respectively) were much larger than those of other samples; consequently, it was not possible to plot the cumulative mass of eroded soil particles of all specimens in an identical graph. These experimental data are marked with an upward arrow symbol in Fig. 8b.

Figure 8 indicates that all of the erosion characteristics of the specimens changed with the concentration of fines in natural soil deposits during seepage tests. The erosion characteristics of specimens classified as CPSS were basically the same as those of specimens composed solely of coarse particles,

**Fig. 7** Onset and progress of internal erosion of companion specimens under different inflow rate. **a** Cumulative mass of eroded soil grains with respect to time. **b** Cumulative mass of eroded particles versus corresponding hydraulic gradient



(a) Cumulative mass of eroded soil grains with respect to time



(b) cumulative mass of eroded particles versus corresponding hydraulic gradient

except for the average hydraulic conductivity, which was profoundly influenced by the fine content when it was less than 30%, as is evident from Fig. 8c. The erosion characteristics of specimens classified as FPSS were nearly the same as those of specimens composed solely of fine particles, except for the

cumulative weight of eroded soil, which was obviously affected by the initial fine content when the concentration of fines was larger than 70% (Fig. 8b). Correspondingly, the erosion characteristics of specimens classified as TCFP varied from those of CPSS to those of FPSS, except for the cumulative

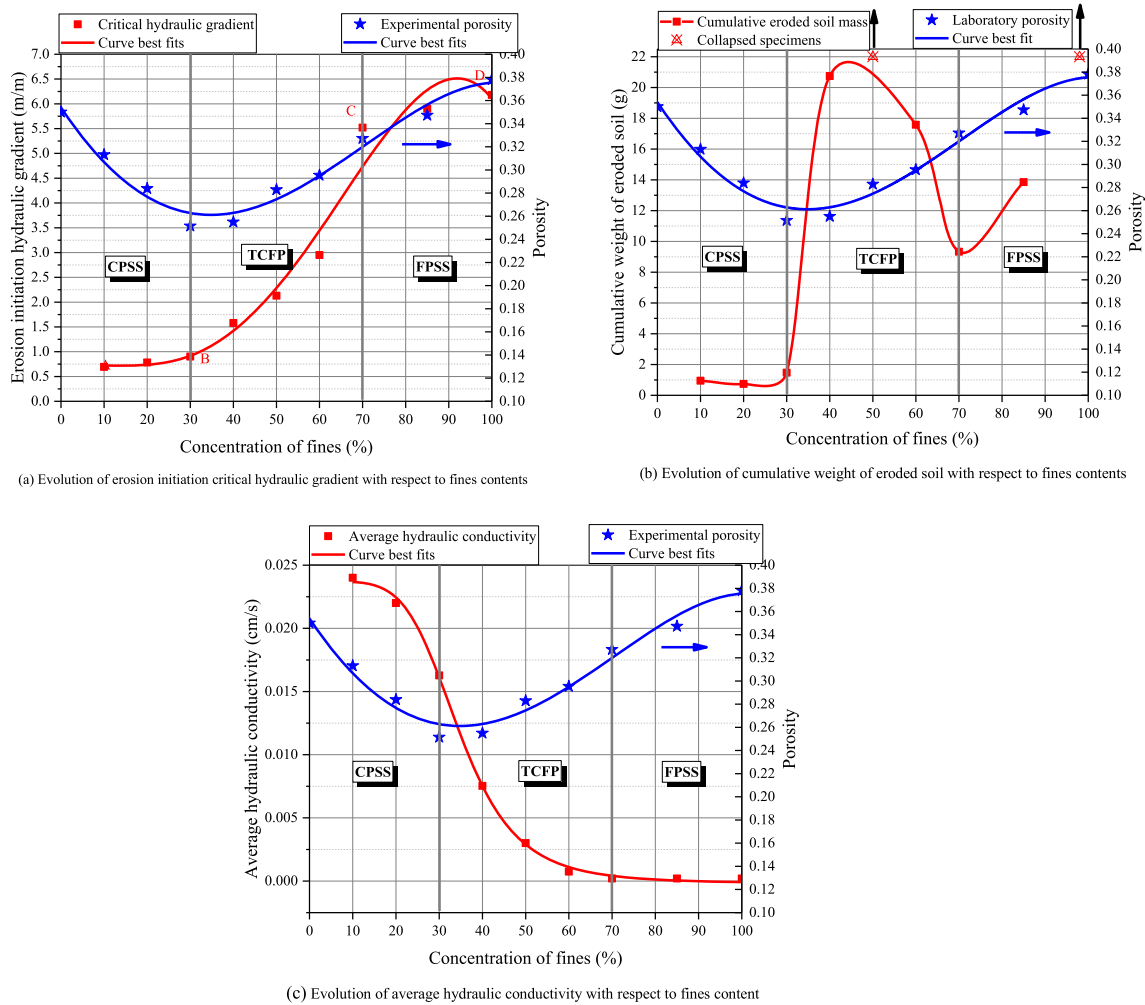


**Fig. 8** Evaluation of erosion characteristics with respect to fines content. **a** Evolution of erosion initiation critical hydraulic gradient with respect to fines content. **b** Evolution of cumulative weight of eroded soil with

respect to fines content. **c** Evolution of average hydraulic conductivity with respect to fines content

mass of eroded soil particles, which is much larger than that of the other granular structures when the concentration of fine particles was between 30 and 70% (Fig. 8b). The distinct difference of erosion characteristics between the three kinds of grain structure confirms that it is reasonable to classify the specimens according to the critical fine contents defined in this contribution.

For specimens classified as CPSS, the growth of fines resulted in an increase of the critical hydraulic gradient of erosion initiation, a minor increase in the cumulative weight of eroded soil, and a decline in porosity and average hydraulic conductivity. It is worth noting that because of unexpected particles loss while nearly cohesionless specimen with fine content of 10% were transferred from the compaction mold to the permeameter cell, the cumulative eroded soil mass was greater than that of specimens with fine content of 20%. It is inferred that in this case, the cumulative eroded soil mass increased with increasing fine contents, once the error is neglected. These results show

that when fine content was less than 30%, higher fine contents and correspondingly lower porosity imply a higher critical hydraulic gradient and greater cumulative eroded soil mass. Based on seepage tests conducted on sand specimens classified as CPSS according to the criteria proposed in this contribution, Ke and Takahashi (2012, 2014b) reported a similar conclusion; that is, specimens with low porosity have low permeability and a high critical hydraulic gradient.

However, the present tests conducted on TCFP and FPSS specimens revealed some opposite results. In contrast to specimens with a CPSS fabric, the growth of fines of TCFP and FPSS specimens resulted in an increase of the critical hydraulic gradient of erosion initiation and porosity, and a decline in average hydraulic conductivity. Specimens with higher porosity had lower coefficients of permeability and higher critical hydraulic gradients.

In fact, pores in the soil are interconnected and continuous. Depending on the fabric, soil particle shape,

and relative compaction, the pore network is intricate and topologically variable. The geometry of pores within soil can be considered as pore bodies with constrictions called pore throats, as defined by Kenney and Lau (1985), shown in Fig. 5a. These pore throats govern the specific permeability of porous media and the transport of particles subsequent to their detachment from pore walls. For each fabric, there were generally two primary groups of pore size: the larger sized group constructed by the coarse soil skeleton and the smaller sized group constructed by fine grains located within the larger pores (Xiao and Shwiyhat 2012). As fines are gradually added into the voids formed by coarse particles, smaller sized pore predominate within the mix, resulting in diminution of the size of pore throats. Diminution of the size of pore throats leads to the more severe inlet hydraulic pressure needed to induce internal erosion. The permeability declines correspondingly even if the overall porosity of the TCFP and FPSS specimens, which is estimated based on Eq. (1), increases with the fine-grain concentration. Such evolution emphasizes the necessity to investigate the effect of the size of pore throats on internal stability instead of the overall porosity. Furthermore, it is essential to distinguish the fabric of specimens prior to investigating the impact of porosity on internal erosion.

It is difficult to evaluate the internal erodibility of specimens with different fabrics solely in reference to the critical hydraulic gradient of erosion initiation or the cumulative eroded soil mass. It can be inferred that the CPSS specimens were most vulnerable to internal erosion, in view of the minimum inlet hydraulic pressure necessary to initiate internal erosion. Specimens with a TCFP fabric were most seriously affected by internal erosion with reference to the maximum cumulative weight of eroded soil particles, even though an intermediate critical hydraulic gradient was needed to activate internal erosion. An efficient argument should be advocated to quantify the internal erodibility of specimens with different fine contents, which is discussed in the “Improved understanding based on critical hydraulic shear stress” section.

### Improved understanding based on shear strength tests

The grain structure schematic depicted in Fig. 5 combined with the change of shear strength developed in specimens with different concentrations of fines exhibited in Fig. 9 could be employed to further elucidate the observations mentioned above. Statistical analysis of the shear strength of specimens with different fabrics subjected to different normal stress is depicted in Table 2.

Finer particles may sit loose in the voids formed by coarse particles, have a considerable role in providing lateral support to the coarse particles, or directly contribute in the soil primary fabric, according to the investigation conducted by Shire et al. (2014). Particles sitting loose in voids, providing lateral support, and contributing in the soil primary fabric are depicted with empty grains, blue grains, and red grains, respectively, in Fig. 5.

Figure 9 and Table 2 indicate the fact that the shear strength and friction angle of CPSS specimens were nearly identical to those of samples composed of coarse particles alone under different normal stress. It is suggested that the coarse particles dominate the internal structure and undertake a major proportion of the load. Fine particles are under relatively small stress as a result. Theoretically, fine particles undertaking the minority of effective stress are easily moved away, independent of the load applied to the specimens and the fine content. Consequently, the critical hydraulic gradient, which is substantially a function of effective stress, is nearly free from the concentration of fines. This inference is in accordance with the conclusions obtained from the erosion characteristics of the CPSS specimens. It was also observed that the growth of fine content results in a tiny increase in shear strength, the contribution of which is mostly from an increase in the friction angle. As fines were progressively added into the voids of the coarse grains in the CPSS specimens, more and more fines started to separate the coarse grains, contributed to the soil primary fabric, and tended not to move as a consequence of the larger contact force on them, as shown in Fig. 5a–c. Correspondingly, a larger fine content allowed for greater fine loss. Therefore, the CPSS specimens with larger fine contents were assumed to show a much larger shear strength, higher critical hydraulic gradient (Fig. 8a), and greater cumulative eroded soil mass (Fig. 8b).

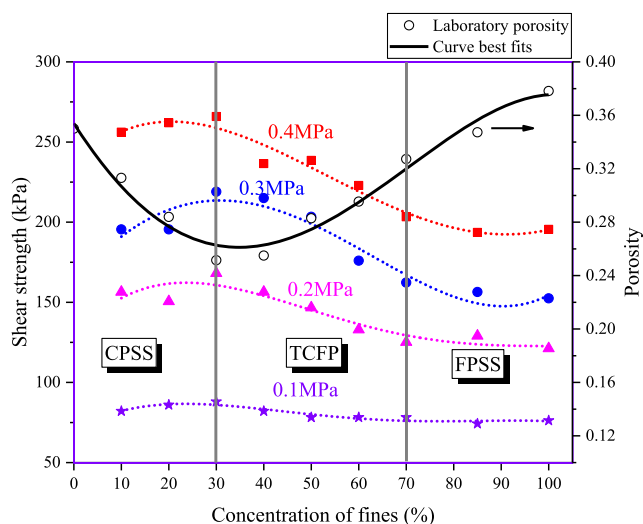


Fig. 9 Change of shear strength developed by specimens with different concentration of fines

**Table 2** Statistical analysis of shear strength of specimens with different fabric subjected to different normal stress

Fines content	Normal stress (kPa)				Cohesive force (kPa)	Friction angle (°)
	100	200	300	400		
Coarse-particle-supported structure	Shear strength (kPa)					
10%	82	156.4	195.5	256.1	32.3	29.4
20%	86.0	150.5	195.5	262.0	30.3	29.8
30%	88.0	168.1	218.9	265.9	34.1	30.3
Transitional coarse–fine-particle-supported structure						
40%	82.1	156.4	215.1	236.5	35.2	27.6
50%	78.2	146.6	203.3	238.5	36.9	28.3
60%	78.2	132.9	176.0	222.8	38.2	25.5
Fine-particle-supported structure						
70%	78.2	125.1	162.3	203.3	39.1	22.4
85%	74.3	129.0	156.4	193.5	42.0	21.1
100%	76.2	121.2	152.5	195.5	41.1	20.6

The shear strength of the FPSS specimens under different normal stress and friction angles was lowest compared with those of the CPSS and TCFP specimens. The cohesion, in contrast, was greatest, as presented in Fig. 9 and Table 2. These results indicate that fine particles within the FPSS specimens shown in Fig. 5e–f govern the structure and properties (i.e., shear strength, critical hydraulic gradient, and hydraulic conductivity). The coarse particles within the FPSS specimens were separated completely by fine particles. Fines are expected to be densely packed and pore throats are expected to be narrow under load action. Consequently, the onset of dislodgement of fines from pore walls and subsequent migration required the highest inlet hydraulic pressure (Fig. 8a). It was also observed that the increase in coarse particle content caused an increase in shear strength. Coarse particles suspended in fine matrix somewhat reinforced the contact of fine particles and prevented the formation of continuous straight seepage passages. Therefore, FPSS specimens with larger coarse-particle content are expected to experience lower fine loss, as presented in Fig. 8b.

The cohesion, friction angle, and shear strength of the TCFP specimens were between those of the CPSS and FPSS specimens. The shear strength of the TCFP specimens seemed to be provided in part by the frictional resistance between a portion of the coarse particles and in part by the frictional resistance between a portion of the fine particles. It is not surprising to observe that the critical hydraulic gradient of the TCFP specimens was between those of the CPSS specimens and FPSS specimens (Fig. 8a). However, it is necessary to underline that the cumulative eroded soil mass was greatest compared with those of the other fabrics (Fig. 8b). In fact, the packing pattern of the interior soil grains within the TCFP specimens was extremely complex, and the pore network was

intricately variable as a result. Continuous weak seepage passages, mostly occupied by unstressed fine particles susceptible to internal erosion as shown in Fig. 5d, probably developed easily. Moreover, the specimens were heterogeneous, and the local velocity field consequently exhibited significant spatial fluctuations. It is possible that the local flow velocity was much higher than the overall macroscopic velocity in some places. Weak seepage passage subjected to violent local flow velocity was assumed to account for the greatest cumulative eroded soil mass observed in the TCFP specimens.

### Improved understanding based on critical hydraulic shear stress

Previously, it has not been possible to reasonably evaluate the ease of initiating erosion in specimens with different fabric types based solely on the critical hydraulic gradient, because of different porosities corresponding to different fine contents. To this end, the critical hydraulic shear stress, another comprehensive indicator of the ease of internal erosion onset, is evaluated in this section.

Flow velocity is the fundamental characteristic responsible for erosion in non-cohesive (Richards and Reddy 2007) and cohesive materials (Arulanandan and Perry 1983). Fines adhering to the pore surface of a soil with relatively high porosity and permeability can be detached and subsequently dislodged by hydrodynamic forces induced by higher flow velocity, if the driving force acting on the fine particles exceeds the critical hydraulic shear stress. It has been demonstrated that it is better to adopt the critical hydraulic shear stress  $\tau_{cr}$ , which is expressed as a function of the intrinsic permeability  $K$  and porosity  $n$ , in addition to the critical hydraulic gradient, to estimate erodibility (Khilar et al. 1985; Reddi et al. 2000). In

the following formula recommended by Reddi et al. (2000), the critical hydraulic shear stress  $\tau_{cr}$  can be calculated:

$$\tau_{cr} = \frac{\Delta P}{\Delta L} \sqrt{\frac{2K}{n}} \quad (3)$$

where  $\Delta P$  is the pressure drop resulting from seepage (Pa);  $\Delta L$  is the height of the specimen (m);  $\frac{\Delta P}{\Delta L}$  is the average hydraulic gradient;  $n$  is the porosity; and  $K$  is the intrinsic permeability ( $\text{m}^2$ ), which is determined by:

$$K = k \frac{\eta}{\gamma_w} \quad (4)$$

where  $k$  is the Darcy coefficient of permeability (m/s),  $\eta$  is the dynamic viscosity ( $\text{kg m}^{-1} \text{s}^{-1}$ ), and  $\gamma_w$  is unit weight of water ( $\text{kN/m}^3$ ).

The evolution of the critical hydraulic shear stress with concentration of fines is plotted in Fig. 10. The critical hydraulic shear stress of TCFP specimens was the lowest, indicating that this fabric was the most prone to undergo internal erosion. In terms of the cumulative eroded soil mass, the TCFP specimens are believed to be most seriously affected by internal erosion. There is no doubt that the internal stability of the TCFP specimens was lowest. As fine particles within the FPSS specimens principally control the structure and properties of the mixture, the critical hydraulic shear stress was independent of fine contents. For the CPSS specimens, the critical hydraulic shear stress slightly increased with growth of fine content, which was attributed to more fines with greater contact force and narrower pore throats. The extent of the impact of fine content on the internal erodibility of the TCFP specimens was much greater than that of the CPSS specimens. These findings underline the necessity to investigate the internal erosion mechanism of TCFP specimens in

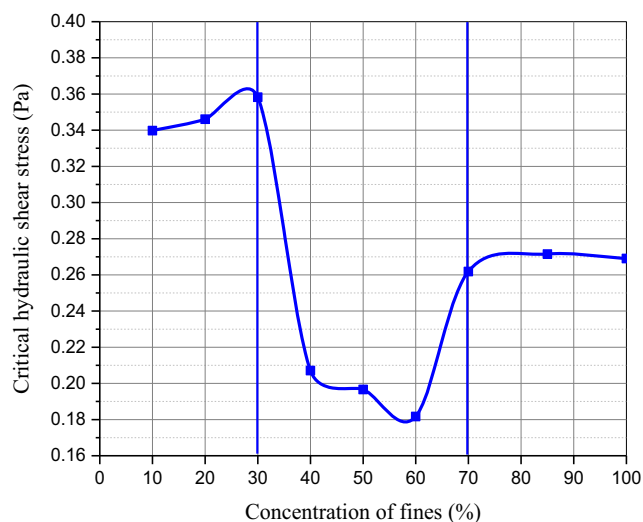


**Fig. 10** Evolution of critical hydraulic shear stress with respect to concentration of fines

addition to those of CPSS specimens reported in previous literature.

## Conclusions

Fine content is a significant factor with respect to the fabric of soil and consequently its internal erodibility. The mechanisms of internal erosion for natural soil deposits with different initial fine contents are presented in this paper. Tested specimens consisted of sandy gravel particles and silty clay particles extracted from original soil. A newly developed fixed-wall permeameter capable of effectively detecting the critical hydraulic gradient of erosion initiation and cumulative weight of eroded soil at a constant inflow rate was presented. Ten kinds of specimens with fine contents ranging from 0 to 100% were prepared for porosity measurement, erosion testing, and direct shear testing. Additionally, erosion tests are performed on four companion specimens to verify the applicability of the apparatus. The following conclusions could be drawn from the laboratory investigation:

- (1) For gap-graded soil, the deficient grain size range can act as a fairly clear division point to divide the mixture into coarse and fine components. There were two significant critical fine contents to classify the grain-supported structure of the mix. It was determined that the specimens could be split into coarse-particle-supported structure (CPSS), transitional coarse-fine-grain-supported structure (TCFP), fine-grain-supported structure (FPSS), based on the critical fine contents of 30% and 70%.
- (2) The internal erosion characteristics of the CPSS specimens were basically the same as those of specimens composed of coarse grains alone. For the coarse-grain-supported structure, larger fine content resulted in lower susceptibility to internal erosion. The internal erodibility of FPSS samples, whose fabric and properties were predominantly controlled by fines, was poorly related to concentration of coarse particles separated thoroughly within the fine matrix. In the fine-supported structure, coarse particles seemed to somewhat reinforce internal stability. It was strongly worthwhile to investigate the internal stability of TCFP, which was most vulnerable to internal erosion. This was verified experimentally based on the minimum critical hydraulic shear stress and maximum cumulative weight of eroded soil.
- (3) For investigating hydromechanical properties such as hydraulic conductivity and erodibility, the laboratory investigation reported in the paper underlines the necessity to depend on average size of pore throats instead of overall porosity. Moreover, the findings in this paper further confirm that critical hydraulic shear stress acts as fundamental characteristics responsible for internal erosion.

**Funding information** The authors acknowledge financial support of the project (2018CDJDTM0006) supported by the Fundamental Research Funds for the Central Universities, the project (KJ-2018024) supported by the Chongqing Planning and Natural Resources Bureau, and the project (KJQN201802501, KJQN201800745) supported by the Scientific and Technological Research Program of Chongqing Municipal Education Commission. We thank Sara J. Mason, MSc, from Liwen Bianji, Edanz Editing China ([www.liwenbianji.cn/ac](http://www.liwenbianji.cn/ac)), for editing the English text of a draft of this manuscript.

## References

- Andrianatrehina L, Souli H, Rech J (2016) Analysis of the internal stability of coarse granular materials according to various criteria. *Eur J Environ Civ Eng* 20:936–953
- Arulanandan K, Perry EB (1983) Erosion in relation to filter design criteria in earth dams. *J Geotech Eng* 109:682–698
- ASTM C117-17 (2018) Standard test method for materials finer than 75- $\mu\text{m}$  (no. 200) sieve in mineral aggregates by washing, Annual book of ASTM standards. ASTM International, West Conshohocken
- ASTM D3080 (2018) Standard test method for direct shear test of soils under consolidated drained conditions, Annual book of ASTM standards. ASTM International, West Conshohocken
- ASTM D4318-17e1 (2018) Standard test methods for liquid limit, plastic limit, and plasticity index of soils, Annual book of ASTM standards. ASTM International, West Conshohocken
- ASTM D698-12e2 (2018) Standard test methods for laboratory compaction characteristics of soil using standard effort (12,400 ft-lbf/ft<sup>3</sup> (600 kN-m/m<sup>3</sup>)), Annual book of ASTM standards. ASTM International, West Conshohocken
- ASTM D854-14 (2018) Standard test methods for specific gravity of soil solids by water pycnometer Annual book of ASTM standards. ASTM International, West Conshohocken
- Bendahmane F, Marot D, Alexis A (2008) Experimental parametric study of suffusion and backward erosion. *J Geotech Geoenviron Eng* 134: 57–67
- Bonelli S (2013) Erosion in geomechanics applied to dams and levees. ISTE Ltd, London
- Burenkova VV (1993) Assessment of suffusion in noncohesive and graded soils. Proc., 1st Int. Conf. Geo-Filters, Karlsruhe, Germany, Balkema, Rotterdam, The Netherlands 357–360
- Chang DS, Zhang LM (2010) Simulation of the erosion process of landslide dams due to overtopping considering variations in soil erodibility along depth. *Nat Hazards Earth Syst Sci* 10:933–946
- Chang DS, Zhang LM (2011) A stress-controlled erosion apparatus for studying internal erosion in soils. *Geotech Test J* 34:579–589
- Chang DS, Zhang LM (2013) Extended internal instability criteria for soils under seepage. *Soils Found* 53:569–583
- Crosta G, di Prisco C (1999) On slope instability induced by seepage erosion. *Can Geotech J* 36:1056–1073
- Dai Z, Huang Y, Xu Q (2019) A hydraulic soil erosion model based on a weakly compressible smoothed particle hydrodynamics method. *Bull Eng Geol Environ* 78:5853–5864
- Fell R, Fry JJ (2013) State of the art on the likelihood of internal erosion of dams and levees by means of testing. In: Bonelli S (ed) Erosion in Geomechanics Applied to Dams and Levees, Chapter 1. ISTE-Wiley, London
- Fell R, Wan CF, Cyganiewicz J, Foster M (2003) Time for development of internal erosion and piping in embankment dams. *J Geotech Geoenviron Eng* 129:307–314
- Foster M, Fell R, Spannagle M (2000) The statistics of embankment dam failures and accidents. *Can Geotech J* 37:1000–1024
- Fragaszy RJ, Su J, Siddiqi FH, Ho CL (1992) Modeling strength of sandy gravel. *J Geotech Eng* 118:920–935
- Frost JD, Park JY (2003) A critical assessment of the moist tamping technique. *Geotech Test J* 26:57–70
- Fry JJ (2012) Introduction to the process of internal erosion in hydraulic structures: embankment dams and dikes. In: Bonelli S (ed) Erosion of Geomaterials, Chapter 1. ISTE-Wiley, London
- Hencher SR (2006) Weathering and erosion processes in rock-implications for geotechnical engineering. In: Proceedings symposium on Hong Kong soils and rocks. 29–79, Institution of Mining, Metallurgy and Materials and Geological Society of London, UK
- Hencher SR (2010) Preferential flow paths through soil and rock and their association with landslides. *Hydrol Process* 24:1610–1630
- Ke L, Takahashi A (2012) Strength reduction of cohesionless soil due to internal erosion induced by one-dimensional upward seepage flow. *Soils Found* 52:698–711
- Ke L, Takahashi A (2014a) Experimental investigations on suffusion characteristics and its mechanical consequences on saturated cohesionless soil. *Geotech Test J* 37:1–18
- Ke L, Takahashi A (2014b) Triaxial erosion test for evaluation mechanical consequences of internal erosion. *Geotech Test J* 54:713–730
- Kenney TC, Lau D (1985) Internal stability of granular filters. *Can Geotech J* 22:420–423
- Kezdi A (1979) Soil physics. Elsevier, Amsterdam
- Khaksar Najafi E, Eslami A (2015) Assessment of the likelihood of suffusion in alluvial soils: case history. *Bull Eng Geol Environ* 74:611–620
- Khilar KC, Fogler HS (1998) Migration of fines in porous media. Springer, Dordrecht
- Khilar KC, Fogler HS, Gray DH (1985) Model for piping-plugging in earthen structures. *J Geotech Eng* 111:833–846
- Ladd RS (1978) Preparing test specimens using undercompaction. *Geotech Test J* 1:1–8
- Liu WP, Wan SF, Huang FM, Luo XY, Fu MF (2019) Experimental study of subsurface erosion in granitic under the conditions of different soil column angles and flow discharges. *Bull Eng Geol Environ* 78:5877–5888
- Luo YL, Qiao L, Liu X, Zhan M, Sheng J (2012) Hydro-mechanical experiments on suffusion under long-term large hydraulic heads. *Nat Hazards* 65:1361–1377
- Mehdizadeh A, Disfani MM, Evans R, Arulrajah A, Ong DEL (2017) Mechanical consequences of suffusion on undrained behaviour of a gap-graded cohesionless soil - an experimental approach. *Geotech Test J* 40:1026–1042
- Mitchell J, Soga K (2005) Fundamentals of soil behavior. Wiley, Hoboken
- Moffat RA, Fannin RJ (2006) A large permeameter for study of internal stability in cohesionless soils. *Geotech Test J* 29:273–279
- Muir Wood D, Maeda K, Nukudani E (2010) Modelling mechanical consequences of erosion. *Géotechnique* 60:447–457
- Ouyang M, Takahashi A (2015) Influence of initial fines content on fabric of soils subjected to internal erosion. *Can Geotech J* 54:713–730
- Pepe G, Filippi D, Cevasco A (2019) First observations on the internal erodibility of some soil-like weathered rocks by means of hole erosion test. *Ital J Eng Geol Environ* 1:93–98
- Reddi LN, Bonala M (1997) Critical shear stress and its relationship with cohesion for sand-kaolinite mixtures. *Can Geotech J* 34:26–33
- Reddi LN, Lee IM, Bonala MVS (2000) Comparison of internal and surface erosion using flow pump tests on a sand-kaolinite mixture. *Geotech Test J* 23:116–122
- Richards KS, Reddy KR (2007) Critical appraisal of piping phenomena in earth dams. *Bull Eng Geol Environ* 66:381–402
- Richards KS, Reddy KR (2010) True triaxial piping test apparatus for evaluation of piping potential in earth structures. *Geotech Test J* 33: 83–95
- Scholtes L, Hicher PY, Sibille L (2010) Multiscale approaches to describe mechanical responses induced by particle removal in granular materials. *CR Mecanique* 338:627–638

- Schuler U (1995) How to deal with the problem of suffusion. Research and Development in the Field of Dams, Switzerland. National Committee on Large Dams, Crans-Montana, pp 145–159
- Shire T, O’Sullivan C, Hanley KJ, Fannin RJ (2014) Fabric and effective stress distribution in internally unstable soils. *J Geotech Geoenviron Eng* 140:04014072
- Skempton AW, Brogan JM (1994) Experiments on piping in sandy gravels. *Geotechnique* 44:449–460
- Slangen P, Fannin RJ (2017) A flexible wall permeameter for investigating suffusion and suffosion. *Geotech Test J* 40:1–14
- Tian DL (2018) Influence factor study of internal stability of silty clay containing rock fragments under Rainfall Infiltration, MPhil. thesis, Chongqing University, Chongqing, China. (In Chinese)
- Vallejo LE (2001) Interpretation of the limits in shear strength in binary granular mixt. *Can Geotech J* 38:1097–1104
- Wan CF, Fell R (2004a) Laboratory tests on the rate of piping erosion of soils in embankment dams. *Geotech Test J* 27:295–303
- Wan CF, Fell R (2004b) Investigation of rate of erosion of soils in embankment dams. *J Geotech Geoenviron Eng* 130:373–380
- Wan CF, Fell R (2008) Assessing the potential of internal instability and suffusion in embankment dams and their foundations. *J Geotech Geoenviron Eng* 134:401–407
- Xiao M, Shwiyhat N (2012) Experimental investigation of the effects of suffusion on physical and geomechanic characteristics of sandy soils. *Geotech Test J* 35:890–900
- Zhang LM, Chen Q (2006) Analysis of seepage failure of the Gouhou rockfill dam during reservoir water infiltration. *Soils Found* 46(5): 557–568
- Zhang LL, Wu F, Zhang H, Zhang L (2019) Influences of internal erosion on infiltration and slope stability. *Bull Eng Geol Environ* 78:1815–1827